Research Article

Preparation, Characterization, and Chemical Stability of Gold Nanoparticles Coated with Mono-, Bis-, and Tris-Chelating Alkanethiols

La-ongnuan Srisombat, Joon-Seo Park, Shishan Zhang, and T. Randall Lee

Langmuir, **2008**, 24 (15), 7750-7754• DOI: 10.1021/la800511g • Publication Date (Web): 12 July 2008

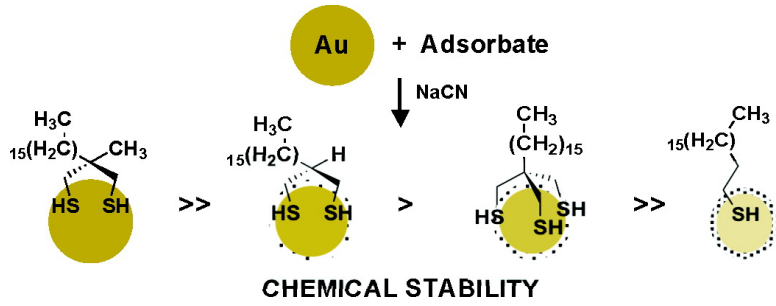

More About This Article

Additional resources and features associated with this article are available within the HTML version:

- Supporting Information
- Links to the 1 articles that cite this article, as of the time of this article download
- Access to high resolution figures
- Links to articles and content related to this article
- Copyright permission to reproduce figures and/or text from this article

View the Full Text HTML

Preparation, Characterization, and Chemical Stability of Gold Nanoparticles Coated with Mono-, Bis-, and Tris-Chelating Alkanethiols

La-ongnuan Srisombat, Joon-Seo Park, Shishan Zhang, and T. Randall Lee*

Departments of Chemistry and Chemical Engineering, University of Houston, 4800 Calhoun Road, Houston, Texas 77204-5003

Received February 18, 2008. Revised Manuscript Received May 2, 2008

A systematically varying series of monolayer-protected clusters (MPCs) was prepared by exposing small gold nanoparticles (∼2 nm in diameter) to the following four adsorbates: *n*-octadecanethiol (***n*-C18**), 2-hexadecylpropane-1,3-dithiol (**C18C2**), 2-hexadecyl-2-methylpropane-1,3-dithiol (**C18C3**), and 1,1,1-tris(mercaptomethyl)heptadecane (***t*-C18**). The resultant MPCs were characterized by solubility studies, UV-vis spectroscopy, transmission electron microscopy (TEM), X-ray photoelectron spectroscopy (XPS), and Fourier-transform infrared spectroscopy (FT-IR). All of the MPCs were soluble in common organic solvents; moreover, analysis by TEM showed that the core dimensions were unaffected by exposure to any of the adsorbates. Separate studies by XPS revealed that the sulfur atoms in all MPCs were predominantly bound to the surface of gold (i.e., ∼85% or better). Analysis by FT-IR showed that MPCs functionalized with ***n*-C18** possessed alkyl chains having the greatest conformational order in both the solid-state and dispersed in solution; in contrast, those generated from the other three adsorbates were more liquid-like with reduced conformational order (or crystallinity). The rate of nanoparticle decomposition induced by cyanide ions was monitored by UV−vis spectroscopy. While MPCs functionalized with ***n*-C18** showed the fastest rate of decomposition, those functionalized with **C18C3** were the most resistant to decomposition. Overall, the following trend in chemical stability was observed, **C18C3** ≫ **C18C2** > ***t*-C18** ≫ ***n*-C18**.

Introduction

In recent years, considerable effort has been devoted to the design and controlled fabrication of nanostructured materials.[1–3] The interest in nanoscale materials stems from the fact that their properties (e.g., optical, electrical, mechanical, and chemical) vary greatly with their size, composition, and morphology.[1] Therefore, effective strategies to build tailored nanomaterials in a reliable and predictable fashion are urgently needed. In particular, metal nanoparticles have been the subject of extensive research due to their potential applications in electronics, catalysis, molecular recognition, and biosensing.[2,3] With the development of alkanethiol adsorption on metal colloids during the past two decades,[4,5] there has been a resurgence of interest in colloidal gold because facile surface modification with a variety of functional groups is possible using simple organosulfur chemistry.[6,7]

Self-assembled monolayers (SAMs) provide a unique opportunity to stabilize metal nanoparticles by isolating them from their environment, where particle growth and agglomeration can be prevented. Studies have shown that SAMs on gold derived from *n*-alkanethiols offer only limited stabilization, which restricts the usefulness of these so-called monolayer-protected clusters (MPCs) in real world applications. Specifically, SAMs derived from *n*-alkanethiols on gold exhibit moderate stability at room temperature[8,9] but decompose rapidly at elevated temperatures in hydrocarbon solvents.[10]

Many strategies have been examined to enhance the stability of SAMs on gold, such as using adsorbates that employ multiple sulfur−gold interactions,[11–13] intermolecular hydrogen bonding,[14] and the incorporation of cross-linking groups within the alkyl chains.[14,15] In particular, the use of chelating adsorbates to bind to the surface of gold can increase SAM stabilities due to the entropy-driven chelate effect.[16,17] Moreover, chelates can be designed[18] to resist the formation of intramolecular disulfides[19,20] upon desorption from the surface.[11,12,20,21]

Our group has been exploring the formation and characterization of SAMs on polycrystalline "flat" gold derived from the adsorption of various chelating alkanethiols,[11,12] where selected prototype structures are shown in Figure 1.[21–25] This research

* To whom correspondence should be addressed. E-mail: trlee@uh.edu.

(1) Daniel, M.-C.; Astruc, D. *Chem. Rev.* **2004**, *104*, 293.
(2) Schmid, G. *Chem. Rev.* **1992**, *92*, 17091.
(3) Brust, M.; Kiely, C. *J. Colloids Surf., A: Physicochem. Eng. Aspects* **2002**, *202*, 175.
(4) Templeton, A. C.; Wuelfing, W. P.; Murray, R. W. *Acc. Chem. Res.* **2000**, *33*, 27.
(5) Balasubramanian, R.; Kim, B.; Tripp, S. L.; Wang, X.; Lieberman, M.; Wei, A. *Langmuir* **2002**, *18*, 3676.
(6) Van Erp, R.; Gribnau, T. C. J.; Van Sommeren, A. P. G.; Bloemers, H. P. J. *J. Immunoassay* **1991**, *12*, 425.
(7) Grabar, K. C.; Smith, P. C.; Musick, M. D.; Dabis, J. A.; Walter, D. G.; Jackson, M. A.; Guthrie, A. P.; Natan, M. J. *J. Am. Chem. Soc.* **1996**, *118*, 1148.
(8) Laibinis, P. E.; Whitesides, G. M. *J. Am. Chem. Soc.* **1992**, *114*, 9022.
(9) Kumar, A. K.; Biebuyck, H. A.; Whitesides, G. M. *Langmuir* **1994**, *10*, 1498.
(10) Bain, C. D.; Troughton, E. B.; Tao, Y.-T.; Evall, J.; Whitesides, G. M.; Nuzzo, R. G. *J. Am. Chem. Soc.* **1989**, *111*, 321.
(11) Garg, N.; Lee, T. R. *Langmuir* **1998**, *14*, 3815.
(12) Garg, N.; Carrasquillo-Molina, E.; Lee, T. R. *Langmuir* **2002**, *18*, 2717.
(13) Wooster, T. T.; Gamm, P. R.; Geiger, W. E.; Oliver, A. M.; Black, A. J.; Graig, D. C.; Paddon-Row, M. N. *Langmuir* **1996**, *12*, 6616.
(14) Clegg, R. S.; Reed, S. M.; Hutchison, J. E. *J. Am. Chem. Soc.* **1998**, *120*, 2486.
(15) Kim, T.; Chan, K. C.; Crooks, R. M. *J. Am. Chem. Soc.* **1997**, *119*, 189.
(16) Purcell, K. F.; Kotz, J. C. *Inorganic Chemistry*; W. B. Saunders: Philadelphia, 1977.
(17) Huheey, J. E. *Inorganic Chemistry*; Harper Collins: Singapore, 1983.
(18) Burns, J. A.; Whitesides, G. M. *J. Am. Chem. Soc.* **1990**, *112*, 6296.
(19) Biebuyck, H. A.; Whitesides, G. M. *Langmuir* **1993**, *9*, 1766.
(20) Kolega, R. R.; Schlenoff, J. B. *Langmuir* **1998**, *14*, 5469.
(21) Shon, Y.-S.; Lee, T. R. *J. Phys. Chem. B.* **2000**, *104*, 8192.
(22) Park, J.-S.; Vo, A. N.; Barriet, D.; Shon, Y.-S.; Lee, T. R. *Langmuir* **2005**, *21*, 2902.
(23) Shon, Y.-S.; Lee, T. R. *J. Phys. Chem. B* **2000**, *104*, 8182.
(24) Shon, Y.-S.; Colorado, R., Jr.; Williams, C. T.; Bain, C. D.; Lee, T. R. *Langmuir* **2000**, *16*, 541.
(25) Park, J.-S.; Smith, A. C.; Lee, T. R. *Langmuir* **2004**, *20*, 5829.

10.1021/la800511g CCC: $40.75
Published on Web 07/12/2008

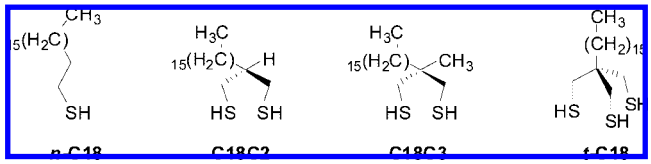

Figure 1. Structures of *n*-octadecanethiol (***n*-C18**), 2-hexadecylpropane-1,3-dithiol (**C18C2**), 2-hexadecyl-2-methylpropane-1,3-dithiol (**C18C3**) and 1,1,1-tris(mercaptomethyl)heptadecane (***t*-C18**).

has recently been expanded to include studies of these SAMs adsorbed on large gold nanoparticles (i.e., diameters ≥ 20 nm), with a focus toward inhibiting the aggregation of these large nanoparticles in solution.[26] When compared to densely packed SAMs generated from normal alkanethiols (***n*-Cn**), SAMs derived from 2-monoalkylpropane-1,3-dithiols (**CnC2**), 2-alkyl-2-methylpropane-1,3-dithiols (**CnC3**), and 1,1,1-tris(mercaptomethyl)-alkanes (***t*-Cn**) exhibited progressively decreasing packing density of alkyl chains in the order of ***n*-Cn** ≫ **CnC2** > **CnC3** > ***t*-Cn**.[21–26] Correspondingly, the degree of conformational order (or crystallinity) of these SAMs was observed to decrease in the same order. Furthermore, thermal desorption studies (on flat gold)[22] and thermally induced aggregation studies (on gold nanoparticles)[26] indicated that the SAMs derived from the tridentate adsorbates (***t*-Cn**) were more thermally stable than those derived from the bidentate adsorbates (**CnC2, CnC3**), which were themselves more stable than the SAMs derived from normal alkanethiols (***n*-Cn**).[21–26] Moreover, ***t*-Cn** molecules were used in independent studies to functionalize gold nanoparticles (∼3 to 5 nm in diameter), where it was found that the bound ***t*-Cn** molecules were resistant to ligand exchange.[27]

In the present study, we wished to examine further the stabilization of gold nanoparticles by chelating alkanethiols, with the specific goal of determining which type of organosulfur ligand best inhibits the cyanide-induced chemical degradation of the metal nanoparticle core. To this end, we functionalized conventional, readily prepared gold nanoparticles (∼2 nm in diameter)[28,29] separately with octadecanethiol (***n*-C18**), 2-hexadecylpropane-1,3-dithiol (**C18C2**), 2-hexadecyl-2-methylpropane-1,3-dithiol (**C18C3**), and 1,1,1-tris(mercaptomethyl)heptadecane (***t*-C18**), whose structures are shown in Figure 1. After fully characterizing these MPCs, we evaluated their relative chemical stability by examining their resistance to etching by cyanide ion.[30]

Experimental Section

Materials. Hydrogen tetrachloroaurate ($HAuCl_4$), toluene, and sodium borohydride ($NaBH_4$) were purchased from EM Sciences. Water was purified to a resistance of 18 MΩ by use of an Academic Milli-Q Water System (Millipore Corporation) and filtered through a 0.22 μm membrane filter before use. Absolute ethanol (Aaper Alcohol), carbon tetrachloride (CCl_4; Acros), tetraoctylammonium bromide (Aldrich), and *n*-octadecanethiol (***n*-C18**; TCI America) were purchased from the indicated suppliers and used as received. The adsorbates 2-hexadecylpropane-1,3-dithiol (**C18C2**), 2-hexadecyl-2-methylpropane-1,3-dithiol (**C18C3**), and 1,1,1-tris(mercaptomethyl)hexadecane (***t*-C18**) were prepared as described previously.[22–25]

Preparation of MPCs Coated with *n*-C18. All glassware was cleaned in aqua regia (3:1, HCl/HNO_3) for at least 1 h, thoroughly rinsed with deionized water and acetone, and then dried in an oven at ∼100 °C prior to use. The monolayer-protected gold nanoparticles were synthesized using a modified Brust−Schiffrin procedure.[28,29] A 2.00 mL aliquot of a 1.0% aqueous solution of $HAuCl_4$ (0.051 mmol) was transferred to a 25 mL round-bottomed flask. A 1.70 mL aliquot of a 7.5×10^{-2} M solution of tetraoctylammonium bromide ($(C_8H_{17})_4NBr$, 0.13 mmol) in toluene was added to the vigorously stirred solution. Stirring was maintained for at least 15 min to ensure complete phase transfer of the gold salt, which was confirmed visually by observing the disappearance of a pale yellow color from the aqueous phase and the appearance of a reddish-orange color to the organic phase. A 0.89 mL aliquot of a 1.9×10^{-2} M solution of *n*-octadecanethiol (0.017 mmol) in toluene was added dropwise to the organic phase. To the vigorously stirred mixture, a 5.72 mL aliquot of a 0.11 M aqueous solution of sodium borohydride (0.63 mmol) was then added dropwise over 15 min. The color of the organic phase immediately changed from reddish-orange to dark violet. The resulting solution was stirred overnight at room temperature. The aqueous phase was removed using a disposable pipet, and the organic phase was concentrated to ∼1 mL by rotary evaporation. The remaining mixture was diluted with 30 mL of absolute ethanol and stored at −50 °C for at least 4 days to induce the functionalized gold nanoparticles to precipitate from the mixture.

Preparation of MPCs Coated with C18C2, C18C3, and *t*-C18. The procedure detailed above was employed with substitution of a 1.05 mL aliquot of a 8.1×10^{-3} M of **C18C2** (0.0085 mmol), a 1.05 mL aliquot of a 8.1×10^{-3} M solution of **C18C3** (0.0085 mmol), or a 0.73 mL aliquot of a 7.7×10^{-3} M solution of ***t*-C18** (0.0056 mmol). The molar ratio of sulfur to gold was maintained at 1:3 for each reaction in order to produce functionalized nanoparticles having similar sizes (i.e., ∼2 nm).

Characterization of MPCs. The size and morphology of the particles were characterized by TEM. To collect the TEM images, a JEOL JEM-2010 electron microscope operating at a bias voltage of 200 kV was used. The samples were prepared by placing small drops of the solutions on a 200 mesh carbon-coated copper grid and allowing the solvent to slowly evaporate at room temperature. The optical properties of the particles were characterized by UV−vis spectroscopy over the range of 300−1100 nm using a Cary 50 scan UV−vis optical spectrometer (Varian) with Cary Win UV software. At room temperature, all samples were placed in a quartz cell having a 1 cm optical path length. The baseline of each spectrum was corrected using the spectrum of the solvent (tetrahydrofuran, THF). Infrared spectra were measured using a Nicolet MAGNA-IR 860 Fourier transform spectrometer. Samples of nanoparticles in solution were analyzed using CCl_4 as the solvent and were recorded using 32 scans. Samples of the nanoparticles in the solid state were prepared by placing a few drops of the nanoparticle solution onto a silicon wafer and allowing the CCl_4 to evaporate. To collect XPS data, we used a PHI 5700 X-ray photoelectron spectrometer equipped with a monochromatic Al Kα X-ray source and PHI 04091 neutralizer. Before introducing the samples into the ultrahigh vacuum (UHV) chamber, each sample was initially dispersed in CCl_4, spotted onto a silicon wafer, and allowed to evaporate to dryness. Standard curve-fitting software (Multipak V5.0A; Physical Electronics, Inc.) using Shirley background subtraction and Gaussian−Lorentzian profiles was used to determine the peak intensities.

Cyanide-Induced Decomposition of MPCs. To a 3 mL solution of MPCs in THF (final concentration ∼1 mM in Au) was added 0.5 mL of aqueous NaCN solution (final concentration ∼8.7 mM) at room temperature. The decay in absorbance at 520 nm was monitored over at least three reaction half-lives by UV−vis spectroscopy. The decomposition rates were analyzed by comparing the initial rates of decomposition, which were fit to a general first-order equation, $y = y' + ae^{-bx}$, where y' is the absorbance due to light scattering by the finely suspended, inorganic reaction byproduct (assumed to be constant).

(26) Zhang, S.; Leem, G.; Srisombat, L.; Lee, T. R. *J. Am. Chem. Soc.* **2008**, *130*, 113.
(27) Wojczykowski, K.; MeiBmer, D.; Jutzi, P.; Ennen, I.; Hutten, A.; Fricke, M.; Volkmer, D. *Chem. Commun.* **2006**, 3693.
(28) Brust, M.; Walker, M.; Bethell, D.; Schiffrin, D. J.; Whyman, R. *J. Chem. Soc., Chem. Commun.* **1994**, 801.
(29) Brust, M.; Fink, J.; Bethell, D.; Schiffrin, D. J.; Kiely, C. *J. Chem. Soc., Chem. Comm.* **1995**, 1655.
(30) Isaacs, S. R.; Cutler, E. C.; Park, J.-S.; Lee, T. R.; Shon, Y.-S. *Langmuir* **2005**, *21*, 5689.

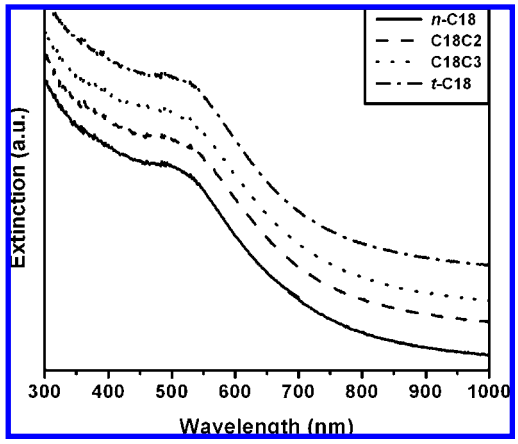

Figure 2. UV−vis spectra of MPCs functionalized with various adsorbates.

Results and Discussion

Solubilities of SAM-Coated Gold Nanoparticles. The solubility of metal nanoparticles in various solvents can be used to monitor the formation of a monolayer on their surfaces.[31,32] Unfunctionalized "bare" gold nanoparticles are well dispersed in water but aggregate in aprotic solvents. In contrast, MPCs functionalized with alkanethiols are insoluble in water but readily disperse in nonpolar aprotic solvents. In the studies reported here, all MPCs coated with ***n*-C18**, **C18C2**, **C18C3**, and ***t*-C18** were prepared as described above, precipitated by centrifugation in ethanol, and then redispersed in the following solvents: hexane, benzene, CCl_4, CH_2Cl_2, and THF. It is important to note that the particles could be successfully redispersed in all of these solvents, but not in water. These observations are consistent with the formation of a monolayer on the surface of the nanoparticles.

UV−Vis Spectroscopy and TEM Images of SAM-Coated Gold Nanoparticles. UV−vis spectroscopy has been used often to characterize the optical properties of functionalized gold nanoparticles (Figure 2).[2,32,33] The extinction maxima of all MPCs were observed at ∼515 nm, corresponding to the plasmon resonance of gold.[30–34] Since the shape and size of the nanoparticles influence the extinction maxima, similar extinction spectra suggest a similar shape and size distribution of nanoparticles for all samples. We confirmed the similarity in size and shape of the MPCs by using TEM as illustrated in Figure 3; histograms showing the respective particle size distributions are included as Supporting Information. Collectively, these data demonstrate that the particles were reproducibly spherical and uniform in size, falling within the expected[28,29] size distribution of 2 ± 1 nm in diameter.

XPS Analysis of SAM-Coated Gold Nanoparticles. The analysis of SAMs on gold by XPS provides insight regarding the atomic composition of the SAMs and the underlying substrate, as well as information regarding the nature of the S−Au interactions.[22,26,31,35–37] Here, we wished to determine whether the sulfur atoms of the ligands were covalently bound to the

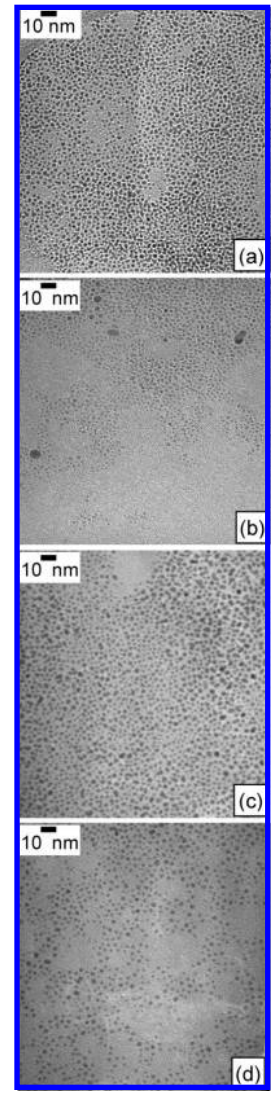

Figure 3. TEM images of MPCs functionalized with (a) ***n*-C18**, (b) **C18C2**, (c) **C18C3**, and (d) ***t*-C18**.

nanoparticle surfaces. For SAMs on flat gold, the sulfur $2p_{3/2}$ signal corresponding to either bound thiol (centered at ∼162 eV) or unbound thiol (centered at ∼163.5 eV) appears as a doublet with a split of 1.2 eV between the peaks.[22,36,37] For all four MPCs prepared here, however, Figure 4 shows that the sulfur $2p_{3/2}$ binding energies were centered at ∼162.5 eV, with no substantial peaks having higher binding energies. Given that the covalent attachment of *n*-alkanethiols to the surface of gold nanoparticles using the experimental approach described here has been established by Raman spectroscopy,[31] we deconvoluted the sulfur spin−orbit doublet using the approach described in the Experimental Section, the results of which indicate that ∼85% or more of all sulfur atoms are bound to the surfaces of the gold nanoparticles. This conclusion is consistent with a recent study exploring the use of chelating ligands to stabilize substantially larger gold nanoparticles.[26] In the present study, it is likely that the peaks are shifted to slightly high binding energy due to sample charging despite use of the aforementioned neutralizer; partial neutralization is a well-known phenomenon in XPS measurements,[38] including the analysis of nanoparticles.[32]

(31) Porter, Jr., L. A.; Ji, D.; Westcott, S. L.; Graupe, M.; Czernuszewicz, R. S.; Halas, N. J.; Lee, T. R. *Langmuir* **1998**, *14*, 7378.
(32) Pham, T.; Jackson, J. B.; Halas, N. J.; Lee, T. R. *Langmuir* **2002**, *18*, 4915.
(33) Asland, K.; Perez-Luna, V. H. *Langmuir* **2002**, *18*, 6069.
(34) Henglein, A. *J. Phys. Chem.* **1993**, *97*, 5457.
(35) Weisbecker, C. S.; Meritt, M. V.; Whitesides, G. M. *Langmuir* **1996**, *12*, 3763.
(36) Johnson, S. R.; Evans, S. D.; Mahon, S. W.; Ulman, A. *Langmuir* **1997**, *13*, 51.
(37) Lu, H. B.; Campbell, C. T.; Castner, D. G. *Langmuir* **2000**, *16*, 1711.
(38) Suzer, S. *Anal. Chem.* **2003**, *75*, 7026.

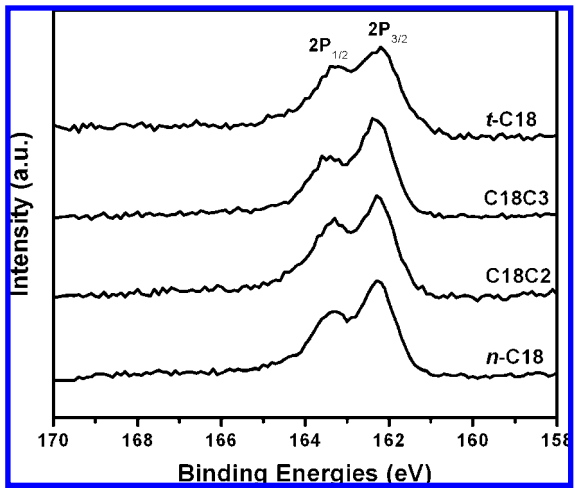

Figure 4. XPS scans of the S 2p region of MPCs deposited on a silicon wafer.

FTIR Analysis of SAM-Coated Gold Nanoparticles. Infrared spectroscopy offers a wealth of information regarding the structure of SAMs on gold nanoparticles, including insight into the order and packing of the alky chains extending away from the surface.[26,28,31] Specially, the C−H stretching region is known to be highly sensitive to the conformation and environment of the alkyl chains as judged by the frequency and width of the absorption bands.[39,40] Furthermore, the position of the $\nu_a^{CH_2}$ band can be used to approximate the degree of conformational order (or crystallinity) of SAMs.[22,24,25,41] In the present study, the conformational order of the alkyl chains of the MPCs was examined for samples dispersed in solution and deposited in solid-state form. Specifically, the MPCs were dispersed in CCl_4 to obtain the conformational order in the liquid state, and MPC solutions were deposited onto a silicon wafer and allowed to dry to obtain the conformational order in the solid state.

As shown in Figure 5 and Table 1, the $\nu_a^{CH_2}$ band of MPCs deposited onto a silicon wafer shift to lower wavenumber when compared to that of MPCs dispersed in solution, suggesting an increase in crystallinity of the sample when measured in the solid state. This trend was observed for MPCs formed from all four adsorbates. The enhanced crystallinity of MPCs in the solid state can plausibly arise from either interdigitation of the tail groups of the alkyl chains attached to neighboring nanoparticles or the loss of solvent molecules from the interchain matrices of individual nanoparticles.[31,32] Previous studies of MPCs, however, showed no evidence for interdigitation in solid-state samples; the increase in crystallinity apparently arises from the loss of solvent. The $\nu_a^{CH_2}$ bands of the MPCs generated from **C18C2**, **C18C3**, and ***t*-C18** appear at a higher wavenumber than that of the MPCs generated from ***n*-C18**, indicating greater disorder for the chains in the former MPCs; similarly, the chains of the **C18C2** MPC appear slightly more ordered than those of the **C18C3** and ***t*-C18** MPCs. The data, however, do not allow us to distinguish the crystallinity of MPCs generated from **C18C3** and ***t*-C18** in either the liquid or the solid state. Overall, the data suggest the following trend in conformational order: ***n*-C18** ≫ **C18C2** > **C18C3** ≈ ***t*-C18**.

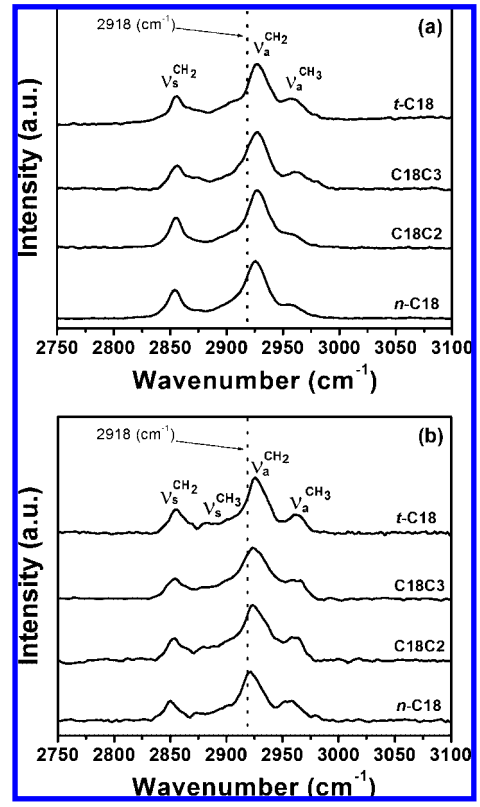

Figure 5. FT-IR transmission spectra in the 2750−3100 cm^{-1} region for MPCs (a) dispersed in CCl_4 and (b) deposited onto a silicon wafer and the CCl_4 allowed to evaporate.

Table 1. Methylene Band Positions (cm^{-1}) of MPCs Dispersed in CCl_4 or Deposited on a Silicon Wafer

MPCs	medium	$\nu_s^{CH_2}$	$\nu_a^{CH_2}$
***n*-C18**	CCl_4	2853	2924
C18C2	CCl_4	2854	2925
C18C3	CCl_4	2854	2925
***t*-C18**	CCl_4	2854	2926
***n*-C18**	Si wafer	2850	2919
C18C2	Si wafer	2852	2923
C18C3	Si wafer	2853	2924
***t*-C18**	Si wafer	2853	2924

NaCN-Induced Decomposition of MPCs. Previous studies of alkanethiolate monolayers on gold nanoparticles have found that one measure of the stability of these systems can be probed by examining their cyanide-induced decomposition.[30,42–44] For MPCs, the rate of decomposition can be monitored by UV−vis spectroscopy, which can be correlated to the extent by which a particular alkanethiolate monolayer provides a protective barrier to the surface of gold. Our studies have found that MPCs generated from ***n*-C18** exhibit two distinct kinetic regimes of decomposition: a fast initial decomposition followed by a slower regime of decomposition. This trend is consistent with that reported in the literature[42,43] and was reproduced here with six independently prepared samples.

To evaluate the rates of decomposition as a function of the structure of the adsorbate, we used only the initial decomposition rates. The observed initial rate constants for the decomposition of MPCs generated from ***n*-C18**, **C18C2**, **C18C3**, and ***t*-C18**

(39) Porter, M. D.; Bright, T. B.; Allara, D. L.; Chidsey, C. E. D. *J. Am. Chem. Soc.* **1987**, *109*, 3559.
(40) Nuzzo, R. G.; Dubois, L. H.; Allara, D. L. *J. Am. Chem. Soc.* **1990**, *112*, 558.
(41) Shon, Y.-S.; Lee, S.; Colorado, Jr., R.; Perry, S. S.; Lee, T. R. *J. Am. Chem. Soc.* **2000**, *122*, 7556.
(42) Templeton, A. C.; Hostetler, M. J.; Kraft, C. T.; Murray, R. W. *J. Am. Chem. Soc.* **1998**, *120*, 1906.
(43) Paulini, R.; Frankamp, B. L.; Rotello, V. M. *Langmuir* **2002**, *18*, 2368.
(44) Agasti, S. S.; You, C. -C.; Arumugam, P.; Rotello, V. M *J. Mater. Chem.* **2008**, *18*, 70.

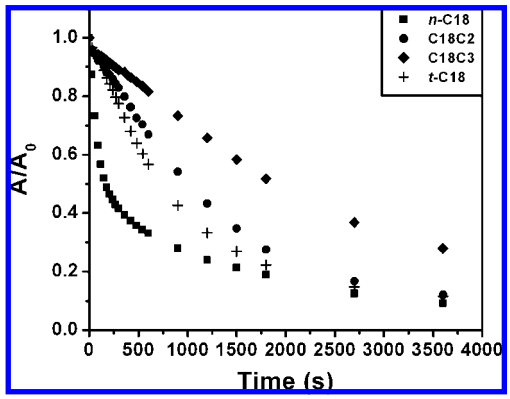

Figure 6. Decomposition profiles of MPCs exposed to NaCN in water.

were 4.8×10^{-3}, 5.8×10^{-4}, 2.7×10^{-4}, and 2.0×10^{-3} s^{-1}, respectively. These values were determined from plots of the initial absorbance decay, $\ln(A_t - A_\infty)$ vs time, which are included as Supporting Information. The data plotted in Figure 6 suggest that the nanoparticles coated with ***n*-C18** decompose significantly faster than those coated with **C18C2**, **C18C3**, and ***t*-C18**. When comparing the latter MPCs, we found that MPCs coated with **C18C3** decompose more slowly than those coated with **C18C2** and ***t*-C18** (i.e., **C18C3** offers the greatest stability). In addition, the rate of decomposition of MPCs derived from ***t*-C18** is somewhat faster than that derived from **C18C2**, giving the following overall trend in stability: **C18C3** ≫ **C18C2** > ***t*-C18** ≫ ***n*-C18**. This observed trend in *chemical* stability was reproducible for at least three independently prepared samples.

Studies have found that the packing density and crystallinity of these four types of SAMs on flat gold[22] and on large gold nanoparticles[26] decrease in the following order: ***n*-Cn** ≫ **CnC2** > **CnC3** > ***t*-Cn**. This trend might also be valid for the MPCs examined here, but the corresponding FT-IR data are less compelling (vide supra), particularly when comparing **C18C3** and ***t*-C18**. We note further that the observed trends in *thermal* decomposition for these types of SAMs on both small[45] and large[26] gold nanoparticles (i.e., ∼2 and ≥20 nm, respectively) and on flat gold[22] inversely follow the documented trend[22,26] in packing density/conformational order (i.e., the most loosely packed adsorbate, ***t*-Cn**, offers the greatest *thermal* stability). The latter observed trend, however, has been rationalized largely on the basis of the chelate effect, where the tris-chelating ligand offers greater stability than the bis-chelating ligands, which in turn offer greater stability than the monochelating ligand.[22,26] Although one might argue that the present crystallinity and stability data are more greatly influenced by surface curvature and defects associated with the small size of the nanoparticle cores, we detect no significant difference in the amount of bound/unbound sulfur on the small gold nanoparticles (vide supra) compared to the large gold nanoparticles[26] for a given adsorbate (i.e., bis-chelates and tris-chelates appear to bind equally well to small and large gold nanoparticles).

To rationalize the trend in *chemical* stability observed here, we propose that the molecular structure of the adsorbate tailgroup plays a critical role together with the chain packing density of the film, as well as the strength of binding between the adsorbate headgroup and the surface of gold. For example, we propose that the film derived from ***n*-C18**, which is undoubtedly the most densely packed and conformationally ordered,[22,26] offers the least protection against chemical degradation because the headgroup is the least strongly bound to the nanoparticle surface, allowing ready ligand desorption and facile etching by cyanide ions. Conversely, the film derived from ***t*-C18**, which is probably the least densely packed but the most strongly bound to the nanoparticle core,[22,26] offers the next least protection because its porous nature allows ready access of cyanide ions to the surface of the nanoparticle and thus facile etching. The remaining ligands, **C18C2** and **C18C3**, appear to offer the greatest protection by providing both strong binding to the nanoparticle core (which inhibits ligand desorption) and moderate interchain packing (which inhibits the access of cyanide ions to the surface of gold via steric/hydrophobic blocking).[42–44]

We are still left to rationalize the enhanced stability afforded by **C18C3** compared to that afforded by **C18C2**. When comparing the molecular structures of these two adsorbates, we propose that the bulky methyl group at the branch position of **C18C3** compared to the hydrogen atom at the **C18C2** branch position impedes the diffusion of cyanide ion to the gold core. This hypothesis is consistent with studies of MPCs coated with highly branched SAMs, which were shown to provide enhanced protection of MPCs when compared to less branched SAMs, giving the following chemical stability order: *sec*-butanethiol > *iso*-butanethiol > *n*-butanethiol.[42] It is also consistent with a more recent study probing the chemical stability of water-soluble MPCs.[44] Taken together, the studies here suggest that a combination of strongly bound headgroups and sterically congested tailgroups are key to promoting the chemical stability of MPCs.

Conclusions

This work has demonstrated the successful preparation of gold nanoparticles coated with ***n*-C18**, **C18C2**, **C18C3**, and ***t*-C18**. The gold cores were ∼2 nm in diameter and monodisperse in shape and size as evaluated by TEM and UV−vis spectroscopy. Analysis by XPS confirmed that the sulfur atoms were predominantly bound to the surface of gold (i.e., ∼85% or better). The crystallinity of the MPCs coated with ***n*-C18**, **C18C2**, **C18C3**, and ***t*-C18** was evaluated using FT-IR spectroscopy, which suggested the following decreasing trend in conformational order for samples both in solution and in the solid state: ***n*-C18** ≫ **C18C2** > **C18C3** ≈ ***t*-C18**. An evaluation of the chemical stability of the MPCs upon exposure to cyanide ion found the following decreasing trend: **C18C3** ≫ **C18C2** > ***t*-C18** ≫ ***n*-C18**. The differences in chemical stability were attributed to a combination of factors, with the two most important being (1) chelation by the sulfur-containing headgroups and (2) enhanced steric bulk of the hydrocarbon tailgroups, where the latter feature impedes the diffusion of cyanide to the underlying gold core.

Acknowledgment We thank the Texas Center for Superconductivity and the Robert A. Welch Foundation (Grant No. E-1320) for generous financial support. We also thank the Royal Thai Government for supporting the predoctoral studies of Ms. Srisombat.

Supporting Information Available: Histograms of the particle size distributions of MPCs and plots of absorbance decay vs time for the cyanide-induced decomposition of MPCs. This material is available free of charge via the Internet at http://pubs.acs.org.

LA800511G

(45) Srisombat, L.; Zhang, S.; Lee, T. R., Results to be published separately.